The Astrophysical Journal, 701:1721–1731, 2009 August 20 doi:10.1088/0004-637X/701/2/1721

SEARCH FOR HIGH-ENERGY MUON NEUTRINOS FROM THE "NAKED-EYE" GRB 080319B WITH THE IceCube NEUTRINO TELESCOPE

R. Abbasi[1], Y. Abdou[2], T. Abu-Zayyad[3], J. Adams[4], J. A. Aguilar[1], M. Ahlers[5], K. Andeen[1], J. Auffenberg[6], X. Bai[7], M. Baker[1], S. W. Barwick[8], R. Bay[9], J. L. Bazo Alba[10], K. Beattie[11], J. J. Beatty[12,13], S. Bechet[14], J. K. Becker[15], K.-H. Becker[6], M. L. Benabderrahmane[10], J. Berdermann[10], P. Berghaus[1], D. Berley[16], E. Bernardini[10], D. Bertrand[14], D. Z. Besson[17], M. Bissok[18], E. Blaufuss[16], D. J. Boersma[1], C. Bohm[19], J. Bolmont[10], O. Botner[20], L. Bradley[21], J. Braun[1], D. Breder[6], T. Castermans[22], D. Chirkin[1], B. Christy[16], J. Clem[7], S. Cohen[23], D. F. Cowen[21,24], M. V. D'Agostino[9], M. Danninger[19], C. T. Day[11], C. De Clercq[25], L. Demirörs[23], O. Depaepe[25], F. Descamps[2], P. Desiati[1], G. de Vries-Uiterweerd[2], T. DeYoung[21], J. C. Diaz-Velez[1], J. Dreyer[15], J. P. Dumm[1], M. R. Duvoort[26], W. R. Edwards[11], R. Ehrlich[16], J. Eisch[1], R. W. Ellsworth[16], O. Engdegård[20], S. Euler[18], P. A. Evenson[7], O. Fadiran[27], A. R. Fazely[28], T. Feusels[2], K. Filimonov[9], C. Finley[1], M. M. Foerster[21], B. D. Fox[21], A. Franckowiak[29], R. Franke[10], T. K. Gaisser[7], J. Gallagher[30], R. Ganugapati[1], L. Gerhardt[9,11], L. Gladstone[1], A. Goldschmidt[11], J. A. Goodman[16], R. Gozzini[31], D. Grant[21], T. Griesel[31], A. Groß[4,32], S. Grullon[1], R. M. Gunasingha[28], M. Gurtner[6], C. Ha[21], A. Hallgren[20], F. Halzen[1], K. Han[4], K. Hanson[1], Y. Hasegawa[33], J. Heise[26], K. Helbing[6], P. Herquet[22], S. Hickford[4], G. C. Hill[1], K. D. Hoffman[16], K. Hoshina[1], D. Hubert[25], W. Huelsnitz[16], J.-P. Hülß[18], P. O. Hulth[19], K. Hultqvist[19], S. Hussain[7], R. L. Imlay[28], M. Inaba[33], A. Ishihara[33], J. Jacobsen[1], G. S. Japaridze[27], H. Johansson[19], J. M. Joseph[11], K.-H. Kampert[6], A. Kappes[1,37], T. Karg[6], A. Karle[1], J. L. Kelley[1], P. Kenny[17], J. Kiryluk[9,11], F. Kislat[10], S. R. Klein[9,11], S. Knops[18], G. Kohnen[22], H. Kolanoski[29], L. Köpke[31], M. Kowalski[29], T. Kowarik[31], M. Krasberg[1], K. Kuehn[12], T. Kuwabara[7], M. Labare[14], S. Lafebre[21], K. Laihem[18], H. Landsman[1], R. Lauer[10], D. Lennarz[18], A. Lucke[29], J. Lundberg[20], J. Lünemann[31], J. Madsen[3], P. Majumdar[10], R. Maruyama[1], K. Mase[33], H. S. Matis[11], C. P. McParland[11], K. Meagher[16], M. Merck[1], P. Mészáros[21,24], E. Middell[10], N. Milke[15], H. Miyamoto[33], A. Mohr[29], T. Montaruli[1,38], R. Morse[1], S. M. Movit[24], K. Münich[15], R. Nahnhauer[10], J. W. Nam[8], P. Nießen[7], D. R. Nygren[11,19], S. Odrowski[32], A. Olivas[16], M. Olivo[20], M. Ono[33], S. Panknin[29], S. Patton[11], C. Pérez de los Heros[20], J. Petrovic[14], A. Piegsa[31], D. Pieloth[15], A. C. Pohl[20,39], R. Porrata[9], N. Potthoff[6], P. B. Price[9], M. Prikockis[21], G. T. Przybylski[11], K. Rawlins[34], P. Redl[16], E. Resconi[32], W. Rhode[15], M. Ribordy[23], A. Rizzo[25], J. P. Rodrigues[1], P. Roth[16], F. Rothmaier[31], C. Rott[12], C. Roucelle[32], D. Rutledge[21], D. Ryckbosch[2], H.-G. Sander[31], S. Sarkar[5], S. Schlenstedt[10], T. Schmidt[16], D. Schneider[1], A. Schukraft[18], O. Schulz[32], M. Schunck[18], D. Seckel[7], B. Semburg[6], S. H. Seo[19], Y. Sestayo[32], S. Seunarine[4], A. Silvestri[8], A. Slipak[21], G. M. Spiczak[3], C. Spiering[10], M. Stamatikos[12], T. Stanev[7], G. Stephens[21], T. Stezelberger[11], R. G. Stokstad[11], M. C. Stoufer[11], S. Stoyanov[7], E. A. Strahler[1], T. Straszheim[16], K.-H. Sulanke[10], G. W. Sullivan[16], Q. Swillens[14], I. Taboada[35], A. Tamburro[3], O. Tarasova[10], A. Tepe[6], S. Ter-Antonyan[28], C. Terranova[23], S. Tilav[7], P. A. Toale[21], D. Tosi[10], D. Turčan[16], N. van Eijndhoven[26], J. Vandenbroucke[9], A. Van Overloop[2], B. Voigt[10], C. Walck[19], T. Waldenmaier[29], M. Walter[10], C. Wendt[1], S. Westerhoff[1], N. Whitehorn[1], C. H. Wiebusch[18], A. Wiedemann[15], G. Wikström[19], D. R. Williams[36], R. Wischnewski[10], H. Wissing[16,18], K. Woschnagg[9], X. W. Xu[28], G. Yodh[8],

and

S. Yoshida[33]

(IceCube Collaboration)

[1] Department of Physics, University of Wisconsin, Madison, WI 53706, USA; kappes@icecube.wisc.edu
[2] Department of Subatomic and Radiation Physics, University of Gent, B-9000 Gent, Belgium
[3] Department of Physics, University of Wisconsin, River Falls, WI 54022, USA
[4] Department of Physics and Astronomy, University of Canterbury, Private Bag 4800, Christchurch, New Zealand
[5] Department of Physics, University of Oxford, 1 Keble Road, Oxford OX1 3NP, UK
[6] Department of Physics, University of Wuppertal, D-42119 Wuppertal, Germany
[7] Bartol Research Institute and Department of Physics and Astronomy, University of Delaware, Newark, DE 19716, USA
[8] Department of Physics and Astronomy, University of California, Irvine, CA 92697, USA
[9] Department of Physics, University of California, Berkeley, CA 94720, USA
[10] DESY, D-15735 Zeuthen, Germany
[11] Lawrence Berkeley National Laboratory, Berkeley, CA 94720, USA
[12] Department of Physics and Center for Cosmology and Astro-Particle Physics, Ohio State University, Columbus, OH 43210, USA
[13] Department of Astronomy, Ohio State University, Columbus, OH 43210, USA
[14] Université Libre de Bruxelles, Science Faculty CP230, B-1050 Brussels, Belgium
[15] Department of Physics, TU Dortmund University, D-44221 Dortmund, Germany
[16] Department of Physics, University of Maryland, College Park, MD 20742, USA
[17] Department of Physics and Astronomy, University of Kansas, Lawrence, KS 66045, USA
[18] III Physikalisches Institut, RWTH Aachen University, D-52056 Aachen, Germany
[19] Oskar Klein Centre and Department of Physics, Stockholm University, SE-10691 Stockholm, Sweden
[20] Department of Physics and Astronomy, Uppsala University, Box 516, S-75120 Uppsala, Sweden
[21] Department of Physics, Pennsylvania State University, University Park, PA 16802, USA
[22] University of Mons-Hainaut, 7000 Mons, Belgium
[23] Laboratory for High Energy Physics, École Polytechnique Fédérale, CH-1015 Lausanne, Switzerland
[24] Department of Astronomy and Astrophysics, Pennsylvania State University, University Park, PA 16802, USA
[25] Vrije Universiteit Brussel, Dienst ELEM, B-1050 Brussels, Belgium
[26] Department of Physics and Astronomy, Utrecht University/SRON, NL-3584 CC Utrecht, Netherlands

[27] CTSPS, Clark-Atlanta University, Atlanta, GA 30314, USA
[28] Department of Physics, Southern University, Baton Rouge, LA 70813, USA
[29] Institut für Physik, Humboldt-Universität zu Berlin, D-12489 Berlin, Germany
[30] Department of Astronomy, University of Wisconsin, Madison, WI 53706, USA
[31] Institute of Physics, University of Mainz, Staudinger Weg 7, D-55099 Mainz, Germany
[32] Max-Planck-Institut für Kernphysik, D-69177 Heidelberg, Germany
[33] Department of Physics, Chiba University, Chiba 263-8522, Japan
[34] Department of Physics and Astronomy, University of Alaska Anchorage, 3211 Providence Dr., Anchorage, AK 99508, USA
[35] School of Physics and Center for Relativistic Astrophysics, Georgia Institute of Technology, Atlanta, GA 30332, USA
[36] Department of Physics and Astronomy, University of Alabama, Tuscaloosa, AL 35487, USA
Received 2009 February 1; accepted 2009 June 25; published 2009 August 4

ABSTRACT

We report on a search with the IceCube detector for high-energy muon neutrinos from GRB 080319B, one of the brightest gamma-ray bursts (GRBs) ever observed. The fireball model predicts that a mean of 0.1 events should be detected by IceCube for a bulk Lorentz boost of the jet of 300. In both the direct on-time window of 66 s and an extended window of about 300 s around the GRB, no excess was found above background. The 90% CL upper limit on the number of track-like events from the GRB is 2.7, corresponding to a muon neutrino fluence limit of 9.5×10^{-3} erg cm^{-2} in the energy range between 120 TeV and 2.2 PeV, which contains 90% of the expected events.

Key words: gamma rays: bursts – methods: data analysis – neutrinos – telescopes

1. INTRODUCTION

Long-duration gamma-ray bursts (GRBs) are thought to originate from the collapse of a massive star into a black hole thereby releasing a huge amount of energy in γ-rays into the surrounding medium. Assuming an isotropic emission of these γ-rays, the measured fluxes yield an isotropic equivalent energy of $\mathcal{O}(10^{52}$–10^{53} erg). However, the actual released energy can be significantly lower if the γ-rays are only emitted within a small cone (jet) as suggested by the observation of signatures for jet breaks in some X-ray spectra. Apart from being amongst the most violent events in the universe, GRBs also belong to the few plausible source candidates for ultra-high-energy cosmic rays. Though our knowledge about GRBs has greatly increased in recent years, their exact nature, the way in which particles are accelerated, and the composition and generation of the jets formed from material accreted onto the black hole are still not fully understood. The observation of high-energy neutrinos from GRBs would be a smoking gun evidence for the acceleration of hadrons in the jets and hence for the connection between GRBs and extra-Galactic cosmic rays.

In the fireball model (Meszaros & Rees 1993), neutrinos of energy $\mathcal{O}(10^{14}$ eV) are produced in the decay of charged pions generated in the interaction of accelerated protons of energy $\mathcal{O}(10^{15}$ eV) with keV–MeV photons via the Δ^+ resonance (Waxman & Bahcall 1997). Both synchrotron and inverse Compton[40] emission from accelerated electrons have been proposed as the mechanism for the production of these photons which form the γ-ray signal measured by satellites. The particle acceleration is thought to occur in internal shocks (Narayan et al. 1992; Rees & Meszaros 1994; Sari & Piran 1997) yielding E^{-2} spectra for protons and electrons as typically expected in *Fermi* acceleration (Waxman & Bahcall 1997). The energy in protons (normalization of the proton spectrum) is usually quoted in relation to the energy in electrons which is linked to the energy in γ-ray photons through the synchrotron and inverse Compton energy-loss mechanisms. In the pion decay neutrinos are produced with the flavor ratios $(\nu_e{:}\nu_\mu{:}\nu_\tau) = (1{:}2{:}0)$,[41] changing to (1:1:1) at the Earth due to oscillations.[42] Their fluence is proportional to the fluence in γ-rays.

The first calculations of the expected neutrino flux from GRBs (Waxman & Bahcall 1997; Alvarez-Muniz & Halzen 1999) used average GRB parameters and the GRB rate measured by BATSE to determine an all-sky neutrino flux from the GRB population. This so-called Waxman–Bahcall GRB flux or similar GRB fluxes have been probed with the AMANDA-II neutrino telescope (Achterberg et al. 2007, 2008) with negative results. These fluxes will be detectable by next-generation neutrino telescopes like IceCube with an instrumented volume of $\gtrsim$1 km^3. However, the average flux for a single burst derived in these models is very small even for km^3 detectors. Nevertheless, as the expected neutrino flux can actually vary by orders of magnitude between GRBs due to fluctuations in the burst parameters (Alvarez-Muniz et al. 2000; Becker et al. 2006), the detection of extremely bright GRBs in neutrinos does seem possible, albeit requiring at least a km^3-size detector, as, for example, was demonstrated in the analysis of GRB 030329 with the AMANDA detector (Stamatikos et al. 2005).

On 2008 March 19, at 06:12:49 UT GRB 080319B (Racusin et al. 2008a) was detected by the *Swift* (Burrows et al. 2005) and Konus-Wind (NASA 1994) satellites at R.A. = 217.°9 and decl. = 36.°3. It was the optically brightest GRB ever observed and with a peak magnitude of 5.3 even visible to the naked eye for a short period of time, despite the fact that the corresponding redshift was about 0.9. It is also one of best measured GRBs with optical wide-field observations covering the whole duration of the explosion (Cwiok et al. 2008) and with many triggered follow-up observations spanning the electromagnetic energy

[37] Also affiliated with Universität Erlangen-Nürnberg, Physikalisches Institut, D-91058, Erlangen, Germany.
[38] On leave of absence from Università di Bari and Sezione INFN, Dipartimento di Fisica, I-70126, Bari, Italy.
[39] Also affiliated with School of Pure and Applied Natural Sciences, Kalmar University, S-39182 Kalmar, Sweden.
[40] Production of γ-rays through inverse Compton emission for bursts with low optical luminosity (majority of bursts) is actually disfavored according to Piran et al. (2009) as it leads to a very high-energy γ-ray component in the TeV range which would carry much more energy than the observed prompt γ-ray emission resulting in an "energy crisis" with most current progenitor models.
[41] Here and throughout the rest of the paper, ν denotes both neutrinos and antineutrinos.
[42] Kashti & Waxman (2005) showed that above a certain energy (typically $\mathcal{O}$(10 PeV)) the ratio changes to (1:1.8:1.8) due to cooling energy losses of the muons producing the neutrinos.

Table 1
Fireball Model Parameters Used in the Calculation of the Neutrino Spectrum for GRB 080319B

Parameter	Value	Reference
$E_\gamma^{\rm iso}$	1.3×10^{54} erg	Racusin et al. (2008a)
Burst duration	66 s	Racusin et al. (2008b)
$\Gamma_{\rm jet}$	300, 500, 1400	Racusin et al. (2008a); see also main text
γ spec.—fluence, $\mathcal{F}_\gamma$ (20 keV–7 MeV)	6.23×10^{-4} erg cm^{-2}	Racusin et al. (2008a)
γ spec.—break energy, ϵ_γ	651 keV	Racusin et al. (2008a) (suppl. information)
γ spec.—1st index, α_γ	0.83	Racusin et al. (2008a) (suppl. information)
γ spec.—2nd index, β_γ	3.5	Racusin et al. (2008a) (suppl. information)
z	0.94	Vreeswijk et al. (2008)
x_π [a]	0.2	Becker (2008)
ϵ_e	0.1	Becker (2008)
ϵ_B	0.1	Becker (2008)
f_e	0.1	Becker (2008)
$t_{\rm var}$	0.01 s	Becker (2008)

Note.
[a] Fraction of proton energy going into pion in a single $p\gamma$ interaction.

spectrum from radio to γ-rays (Racusin et al. (2008a) and references therein).

2. NEUTRINO SPECTRUM CALCULATION

We calculate the expected prompt neutrino spectrum for GRB 080319B in the internal shock scenario of the fireball model following Guetta et al. (2004) which is based on Waxman & Bahcall (1997). This model allows for the easy incorporation of many measured parameters of GRB 080319B (in Waxman & Bahcall (1997) average GRB parameters are used) which is crucial when investigating a GRB that deviates largely from the average GRB. Other models like Murase & Nagataki (2006)[43] or Razzaque et al. (2003) do not provide this possibility without obtaining the actual simulation code and are therefore not considered here.

For reference, we list all formulae used in our calculations in Appendix A. One of the major inputs to the model is the keV–MeV γ-ray spectrum recorded by the satellites. In contrast to Guetta et al. (2004) where a broken power law was used, we parameterize the γ-ray spectrum with a Band function (Band et al. 1993; Equation (A2)). The function parameters obtained from a fit to the time integrated Konus-Wind spectrum are taken from Racusin et al. (2008a) (suppl. information) and are listed in Table 1. The table also contains additional parameters with their values required by the model. Not all of them are measured or even well known. For the jet parameters ϵ_e (fraction of jet energy in electrons), ϵ_B (fraction of jet energy in magnetic field) and f_e (ratio between energy in electrons and protons) typical values of 0.1 are used (Becker 2008). The variability of the γ-ray flux $t_{\rm var}$, which is used as a measure for the time between the emission of two consecutive shells, was analyzed in Margutti et al. (2008). They find an initial timescale of 0.1 s which increased to 0.7 s in the course of the emission. However, their analysis was limited to the energy range between 15 and 150 keV, where for high energies (100–150 keV) the dominant timescale was significantly shorter (0.05 s). By contrast, muons reconstructed in the IceCube detector are mainly produced by neutrinos near the first break energy (Figures 1 and 5(b)) which originate from proton interactions with γ-rays around 500 keV (break energy in γ-ray spectrum). Due to the large gap between 150 and 500 keV and the lack of an extrapolation method, we use a typical value of $t_{\rm var} = 0.01$ s (Becker 2008) in our calculations.

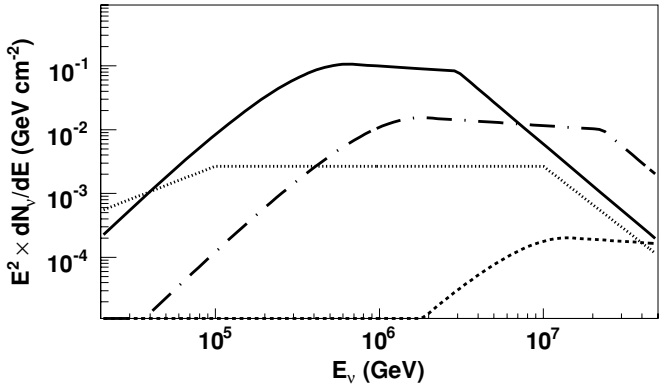

Figure 1. Calculated muon neutrino spectrum for different bulk Lorentz boost factors $\Gamma_{\rm jet}$ of the GRB jet: $\Gamma_{\rm jet} = 300$ (solid line), $\Gamma_{\rm jet} = 500$ (dash-dotted line), and $\Gamma_{\rm jet} = 1400$ (dotted line). For comparison, the average Waxman–Bahcall GRB fluence for a single GRB is also shown (fine-dotted line).

The neutrino spectrum is parameterized as a Band function with a broken power law at high energies (Equation (A5)), where the latter describes the steepening of the spectrum due to synchrotron losses of pions and muons. The energy in neutrinos, i.e., the normalization of the spectrum, is proportional to f_e^{-1} and the energy in γ-ray photons (Equation (A10)). The $\Gamma_{\rm jet}$ factor, which enters the model equations to the second and fourth power (Equations (A6), (A7), and (A9)), has a large impact on the normalization of the neutrino fluence. With increasing $\Gamma_{\rm jet}$, the shell collisions occur at larger distances from the black hole where the photon field and hence the target density for the pion production is smaller. The value of $\Gamma_{\rm jet}$ can be estimated from the fact that the source has to be transparent for γ-rays near the maximum γ-ray energy produced (Guetta et al. 2004). Using the parameters given in Table 1 and a maximum γ-ray energy of 100 MeV yields $\Gamma_{\rm jet} \approx 300$. In Racusin et al. (2008a), the authors argue that the exceptional brightness of the optical flash in GRB 080319B implies that the self-absorption frequency cannot be far above the optical band and they determine $\Gamma_{\rm jet}$ to lie between 300 and 1400. Pandey et al. (2009) obtain $\Gamma_{\rm jet} \approx 300$ from an extrapolation of the late-time evolution of the afterglow. Using a synchrotron self-Compton model, Kumar & Panaitescu (2008) find a $\Gamma_{\rm jet}$ factor of $\sim$500. For the calculation of the neutrino

[43] This model is actually similar to Waxman & Bahcall (1997) but uses Monte Carlo simulation to calculate the photomeson production in $p\gamma$ interactions and takes the synchrotron losses of mesons and protons into account.

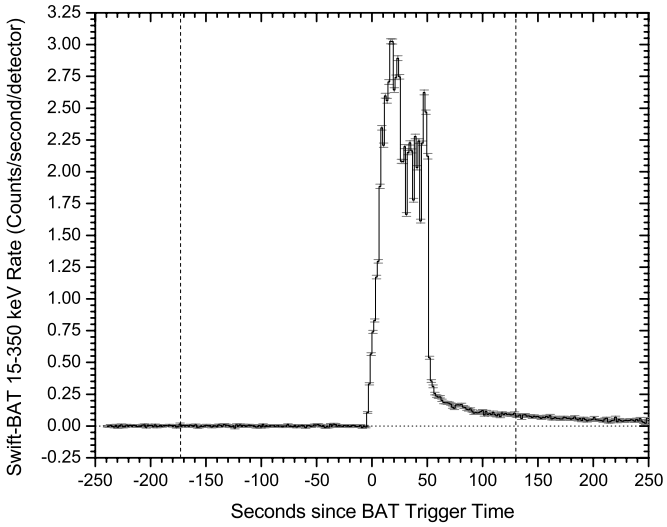

Figure 2. γ-Ray emission from GRB 080319B as measured by *Swift*-BAT (M. Stamatikos 2008, private communication) with T_0 = 06:12:49 UT. The dashed vertical lines mark the time range covered by IceCube data.

spectrum, we adopt the optimistic case with $\Gamma_{\rm jet} = 300$ which is displayed in Figure 1 as the solid line. An increase of the $\Gamma_{\rm jet}$ factor to 500 (1400) decreases the neutrino fluence by about a factor 10 (10^3) and shifts it to higher energies (Figure 1 dashed and dotted lines). Muon cooling (Kashti & Waxman 2005) affects the neutrino spectrum only at energies above ~20 PeV ($\Gamma_{\rm jet} = 300$) and is therefore negligible for our analysis.

3. ANALYSIS OF IceCube DATA

IceCube (Achterberg et al. 2006), the successor of the AMANDA experiment and the first next-generation neutrino telescope, is currently being installed in the deep ice at the geographic South Pole. Its final configuration will instrument a volume of about 1 km^3 of clear ice in depths between 1450 m and 2450 m. Neutrinos are reconstructed by detecting the Cherenkov light from charged secondary particles, which are produced in interactions of the neutrinos with the nuclei in the ice or bedrock. The optical sensors consist of photomultipliers housed in pressure-resistant glass spheres (digital optical modules (DOMs); Abbasi et al. 2009) which are mounted on vertical strings. Each string carries 60 DOMs with the final detector containing 80 such strings. Physics data taking with IceCube started in 2006 with nine strings installed. At the beginning of 2007, the detector was enlarged to 22 strings. Since 2009 April, IceCube has been running with 59 strings. The completion of the detector construction is planned for the year 2011.

3.1. Data Sets, Event Reconstruction, and Selection

The data acquisition (DAQ) system of IceCube (Abbasi et al. 2009) is based on local coincidences between neighboring DOMs in a string within 1 μs for which the photon signal passes a threshold of 0.4 photoelectrons. All data from DOMs belonging to a local coincidence are read out and the digitized waveforms are sent to a computer farm at the surface. In order to pass the trigger, a minimum number of eight DOMs in local coincidences within a time window of 5000 ns is required. If this condition is fulfilled, the waveforms are combined to an event and the number and arrival times of the Cherenkov photons are extracted. For each event, an initial track is reconstructed using the line-fit algorithm (Ahrens et al. 2004). This is a simple but fast track reconstruction based on the measured hit times in the DOMs. We do not consider events where only a shower is produced (e.g., in interactions of electron neutrinos or neutral current neutrino interactions) as only the track-like light pattern of muons allows for a good angular resolution. Hence, this search focuses on muon neutrinos from GRB 080319B. Cuts on the reconstructed zenith angle ($>70^\circ$) and number of hit DOMs (>10) reject downgoing atmospheric muons and reduce the event rate down to the 117 Hz. This allows to apply more advanced reconstruction algorithms to the remaining neutrino candidates. A more precise estimate of the direction of a neutrino candidate is obtained by fitting a muon-track hypothesis to the pattern of the recorded Cherenkov light in the detector using a log-likelihood reconstruction method (Ahrens et al. 2004). A fit of a paraboloid to the region around the minimum of the log-likelihood function yields an estimate of the uncertainty on the reconstructed direction. The absolute time of an event is determined with a GPS clock with a precision of better than a millisecond, which is more than sufficient for this analysis.

At the time of GRB 080319B, IceCube was running in maintenance mode with 9 out of 22 strings taking data. Apart from the reduced number of strings, the DAQ system had a slightly different configuration than during normal operation. IceCube data are available in a window of about 300 s around the GRB (on-time data) as displayed in Figure 2. The detector was checked for stability during this period by plotting the rate of events passing the trigger in bins of time, R, relative to the average rate $\tilde{R}$ of 117 Hz (Figure 3). The variations in the event rate are compatible with statistical fluctuations and there were no indications for abnormal behavior of the detector during the period under consideration.

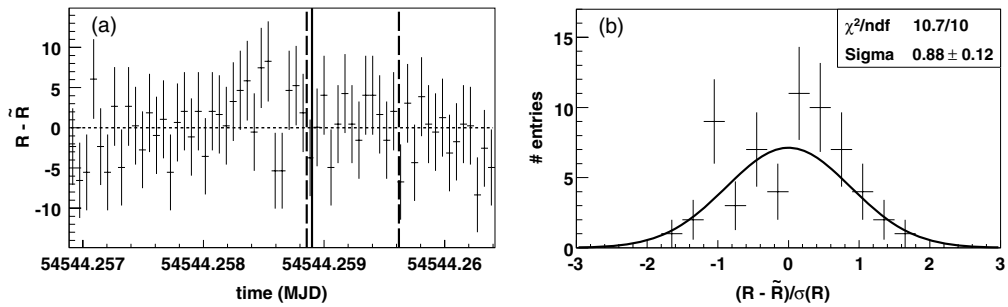

Figure 3. (a) Difference between the event rate in a 5 s bin, R, and the average rate $\tilde{R}$ (calculated from all events in the 300 s time window shown) as a function of time at trigger level. The solid and dashed vertical lines mark the satellite trigger time of the GRB and the start and stop times of the measured γ-ray emission, respectively. (b) Histogram of $(R - \tilde{R})$ divided by the statistical errors. The line is a fit of a Gaussian distribution to the histogram.

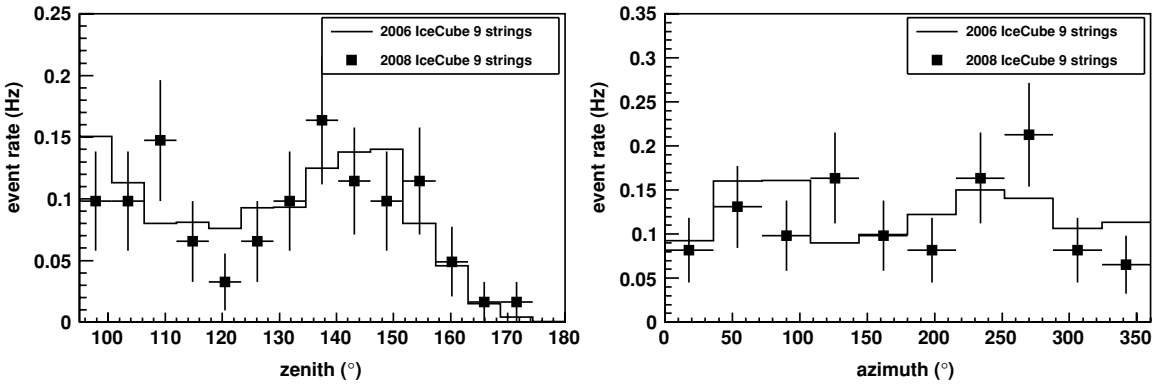

Figure 4. Comparison after quality cuts (Equation (1)) of the background data set (2006 IceCube 9 strings) with a 1 hr data set taken 1 week after GRB 080319B with equivalent DAQ settings (2008 IceCube 9 strings).

Table 2
Number of Expected Signal and Background Events at Different Cut Levels

Cut Level	Signal		Background (Off-Time Data)		Comment
	No. Events	Efficiency[a] (%)	No. Events[b]	Efficiency[a] (%)	
Trigger	0.24	100	1.2×10^{-1}	100	See Section 3.1
Quality	0.14	58	1.4×10^{-3}	1.2	See Equation (1)
Final	0.10	41	1.7×10^{-5}	0.014	See Equation (2)

Notes.
[a] Relative to trigger level.
[b] In a cone with radius 5° centered on GRB 080319B position within 66 s.

In order to avoid systematic uncertainties due to inaccuracies in the simulation when calculating the significance of a deviation from the background-only hypothesis, the expected background in the on-time window is determined from the observed off-time data. However, the amount of data taken with the special DAQ configuration during the regular maintenance runs is limited and not sufficient for a good background estimation. Instead, we utilize the IceCube data set of the 2006 data taking period (131 days lifetime), when the detector consisted only of the same nine strings which were taking data during GRB 080319B. After applying the following quality cuts, the 2006 data set shows good agreement with the GRB 080319B maintenance data set (Figure 4)

$$\theta_{\rm rec} > 90^\circ; \quad \sigma_{\rm dir} < 10^\circ; \quad \theta_{\rm min} > 70^\circ;$$

$$L_{\rm red} \leqslant \begin{cases} 9.0 & \text{for} \quad 4 \leqslant N_{\rm dir} \leqslant 10 \\ 8.0 & \text{for} \quad N_{\rm dir} < 4 \end{cases} \tag{1}$$

with

1. $\theta_{\rm rec}$: reconstructed zenith angle;
2. $\sigma_{\rm dir}$: uncertainty on the reconstructed track direction (quadratic average of the minor and major axis of the 1σ error ellipse);
3. $L_{\rm red}$: $-\log_{10}$ of the likelihood value of the reconstructed track divided by the number of degrees of freedom (number of hit DOMs minus number of fit parameters). In conjunction with the selection of upgoing tracks, it has proven to be an efficient variable for separating upgoing atmospheric neutrinos from misreconstructed downgoing atmospheric muons. It exploits the fact that for a light pattern originating from a downgoing muon the incorrect upgoing track hypothesis yields rather low likelihood values;
4. $N_{\rm dir}$: number of photons detected within a −15 to +75 ns time window with respect to the expected arrival time for unscattered photons from the muon-track hypothesis; and
5. $\theta_{\rm min}$: minimum of the two zenith angles from a fit of a two-track hypothesis to the light pattern.

The $\theta_{\rm min}$ cut rejects events where two downgoing muons from independent atmospheric showers pass through the detector in quick succession and produce a light pattern that fakes an upgoing track. The difference in the overall rates of the two samples is about 10% which is within the statistical error of the total number of events in the maintenance data set.

For the final analysis, we use the method described in Section 3.3 to maximize the potential for a discovery: the cuts on $\sigma_{\rm dir}$ and $N_{\rm dir}$ are tightened until we reach a maximum in the probability to detect the fluence calculated in Section 2 ($\Gamma_{\rm jet} = 300$) with a significance of at least 4σ. In order to avoid biasing the results, only the off-time data are used and the on-time data are kept "blind" during this procedure. The optimized cuts are

$$\theta_{\rm rec} > 90^\circ; \quad \sigma_{\rm dir} < 5^\circ; \quad \theta_{\rm min} > 70^\circ;$$

$$L_{\rm red} \leqslant \begin{cases} 9.0 & \text{for } 8 \leqslant N_{\rm dir} \leqslant 10 \\ 8.0 & \text{for } N_{\rm dir} < 8 \end{cases} . \tag{2}$$

After these cuts, the data sample with an event rate of about 5×10^{-2} Hz is still dominated by misreconstructed downgoing muons (a Monte Carlo simulation of atmospheric neutrinos yields an event rate of 2×10^{-3} Hz). For a search cone with 5° radius centered on the GRB position and a time window of 66 s, a mean number of background events of 1.7×10^{-5} is expected. A summary of the event rates at different cut levels is given in Table 2.

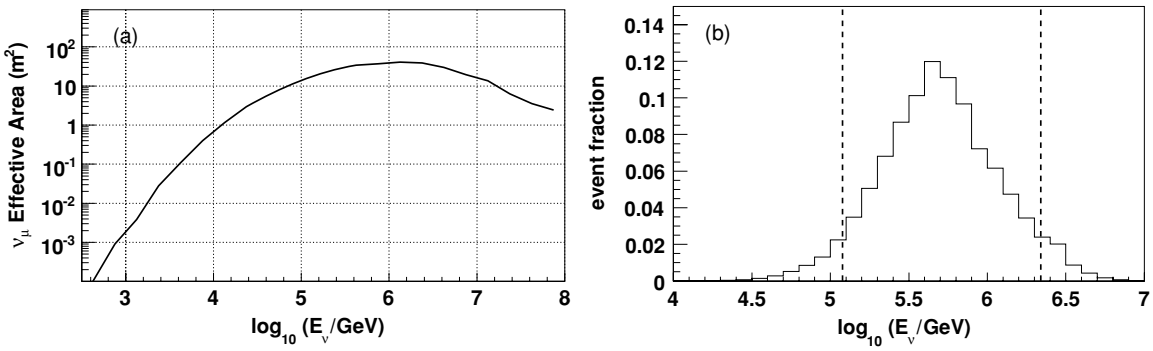

Figure 5. (a) Effective area at final cut level for muon neutrinos from the direction of GRB 080319B as a function of the neutrino energy. (b) Expected mean number of Monte Carlo signal events after final cuts as a function of neutrino energy. The two vertical lines mark the central interval containing 90% of the events.

3.2. Monte Carlo

Signal muon neutrinos from GRB 080319B are generated with a Monte Carlo and weighted according to the fluence calculated in Section 2. The Monte Carlo contains a detailed simulation of the propagation of the muon neutrino through the Earth and the ice using the ANIS generator (Gazizov & Kowalski 2005). After the interaction, the muon is traced through rock and ice taking into account continuous and stochastic energy losses (Chirkin & Rhode 2004). The photon signal in the DOMs is determined from a detailed simulation (Lundberg et al. 2007) of the propagation of Cherenkov light through the ice which includes the modeling of the changes in absorption and scattering length with depth (Ackermann et al. 2006). This is followed by a simulation of the DOM electronics and the trigger. The DOM signals are then processed in the same way as the real data. Background events do not have to be simulated as these are taken from off-time data.

After final cuts (Equation (2)) and for neutrinos from the direction of the GRB (weighted according to the calculated GRB spectrum), 90% of all reconstructed Monte Carlo tracks are contained within 20° of the true direction. The median angular resolution is 5.°6. This resolution is worse than the one usually quoted for IceCube in its nine-string configuration for neutrino-induced muons. The reason for this is that the geometry of the detector was such that the reconstruction lever arm was at its shortest for the direction of GRB 080319B. The corresponding muon neutrino effective area as a function of energy is displayed in Figure 5(a). The expected mean number of events from the GRB ($\Gamma_{\rm jet} = 300$) after final cuts is 0.1, with 90% of the events contained in the energy range from 120 TeV to 2.2 PeV (Figure 5(b)). A summary of the event rates at different cut levels is given in Table 2.

In order to compare the signal (neutrino) Monte Carlo to data, a high-purity (atmospheric) muon neutrino sample from the off-time data is selected by requiring zenith $>100^\circ$, $\sigma_{\rm dir} < 2.^\circ5$, and $N_{\rm dir} > 8$ (these tight cuts are only used for this comparison and not in the following analysis of the data). Figure 6 shows good agreement between data and the Monte Carlo weighted to the atmospheric muon neutrino flux of Barr et al. (2004; Bartol spectrum).

3.3. Unbinned Likelihood Analysis

The final analysis is based on data sets at final cut level (Equation (2)). The data are analyzed using an unbinned log-likelihood method similar to the one described in Braun et al. (2008). In contrast to binned methods where the event is rejected if it lies outside the cut region (binary selection), unbinned likelihood methods do not throw away events but use probability density functions (PDFs) to evaluate the probability of an event to belong to signal or background. Therefore, they are more powerful than binned methods.

In the case of searches for neutrinos from GRBs detected by satellites, the direction and time of reconstructed tracks are the most crucial information to separate signal from background. Hence, both the signal, $S(\vec{x}_i)$, and background, $B(\vec{x}_i)$, PDFs are each the product of a time PDF and a directional PDF, where $\vec{x}_i$ denotes both the directional and time variables. The directional signal PDF is a two-dimensional Gaussian distribution with the two widths being the major and minor axis of the 1σ error ellipse of the paraboloid fit described in the previous section. The time PDF is flat over the γ-ray emission time and falls off on both sides with a Gaussian distribution with $\sigma = 25$ s. The Gaussian accounts for possible small shifts in the neutrino emission time with respect to that of the γ-rays and prevents discontinuities in the likelihood function. The sensitivity of the analysis depends only weakly on the exact choice of σ, e.g., the quoted upper limit changes by less than 2% when doubling σ. For the directional background PDF, the detector asymmetries in zenith and azimuth have to be taken into account. This is accomplished by evaluating the data in the detector coordinate system. The directional background PDF is hence derived from the distribution of all background events after final cuts in the zenith–azimuth plane of the detector. The time distribution of background tracks during the GRB can be assumed to be constant resulting in a flat time PDF.

Both PDFs are combined in an extended log-likelihood function (Barlow 1989)

$$\ln\left(\mathcal{L}(\langle n_s\rangle)\right) = -\langle n_s\rangle - \langle n_b\rangle + \sum_{i=1}^{N} \ln\left(\langle n_s\rangle\, S(\vec{x}_i) + \langle n_b\rangle\, B(\vec{x}_i)\right), \tag{3}$$

where the sum runs over all reconstructed tracks left after cuts with $\vec{x}_i$ representing the PDF parameters (absolute time of the track along with the track direction in local detector coordinates and its estimated uncertainty). The variable $\langle n_b\rangle$ is the expected mean number of background events, which is determined from the background data set. The mean number of signal events, $\langle n_s\rangle$, is a free parameter which is varied to maximize the expression

$$\ln\left(\mathcal{R}(\langle n_s\rangle)\right) = \ln\left(\frac{\mathcal{L}(\langle n_s\rangle)}{\mathcal{L}(0)}\right) = -\langle n_s\rangle + \sum_{i=1}^{N} \ln\left(\frac{\langle n_s\rangle\, S(\vec{x}_i)}{\langle n_b\rangle\, B(\vec{x}_i)} + 1\right) \tag{4}$$

in order to obtain the best estimate for the number of signal events, $\langle \hat{n}_s\rangle$.

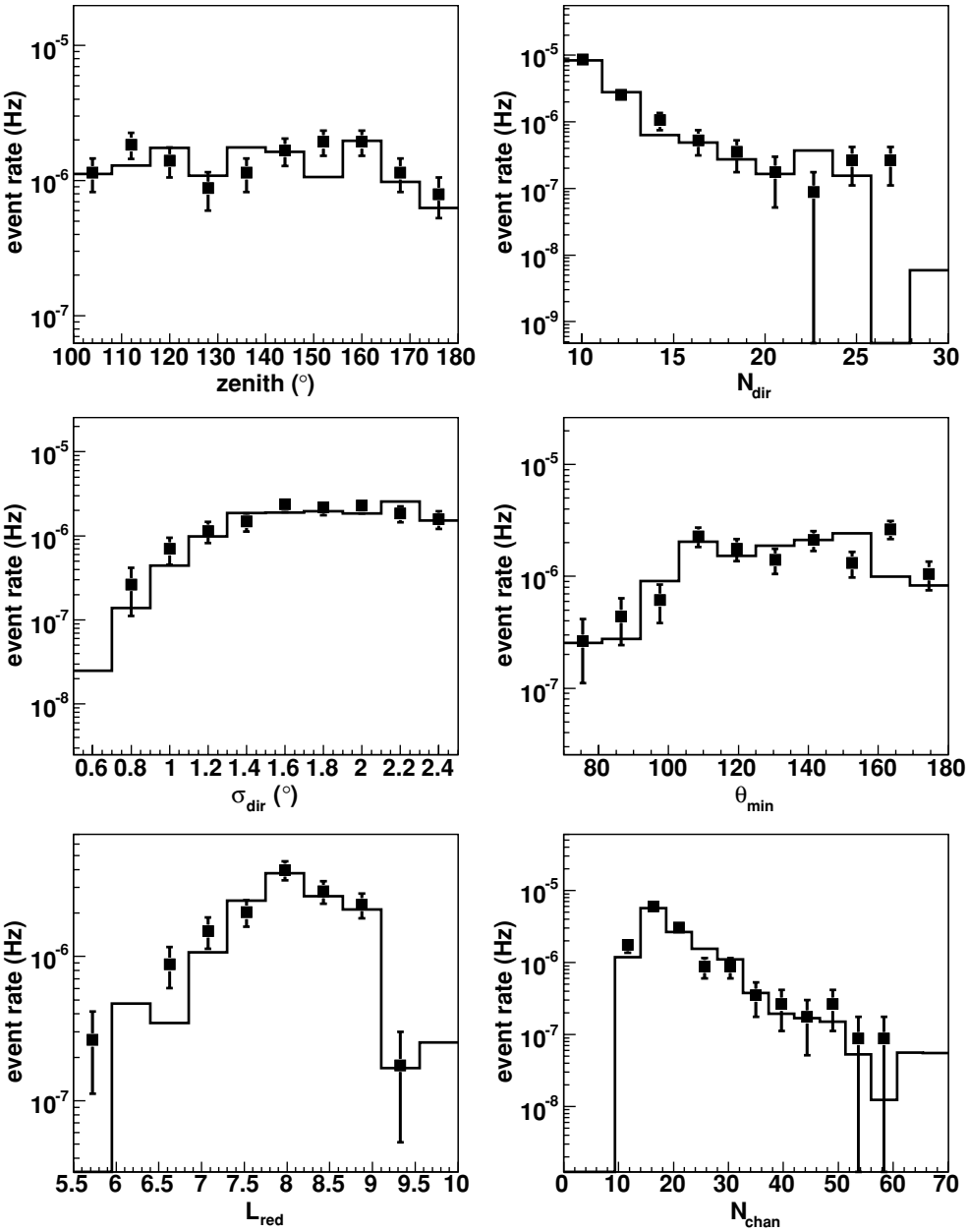

Figure 6. Comparison between an atmospheric muon neutrino Monte Carlo (solid line) and a high-purity data set of (atmospheric) muon neutrinos (filled squares) in different variables.

To determine whether a given data set is compatible with the background-only hypothesis, a large number of background data sets for the on-time window are generated from the 2006 nine-string data by randomizing the track times while taking into account the downtime of the detector. For each of these data sets, the $\ln(\mathcal{R})$ value is calculated, yielding the distribution shown in Figure 7(a). The probability for a data set to be compatible with background is given by the fraction of background data sets with an equal or larger $\ln(\mathcal{R})$ value (p-value). The sensitivity of the IceCube detector to neutrinos from GRB 080319B is determined by injecting different numbers of Monte Carlo signal events into the generated randomized background data sets and calculating the resulting p-value (see Figure 7(a)).

GRBs are expected to generate a substantially harder neutrino energy spectrum than that of atmospheric neutrinos. A detector quantity closely related to the neutrino energy is the number of DOMs (channels) with detected photons, $N_{\rm chan}$. This quantity is used to enhance the sensitivity to a possible signal. Figure 7(b) shows the $N_{\rm chan}$ distribution of off-time data events within a cone with 20° radius centered on the GRB position (no events remain in the on-time data set) together with a signal Monte Carlo which has been normalized to the number of data events. Combining this information with the p-value from the $\ln(\mathcal{R})$ distribution increases the detection probability. The potential for discovering a muon neutrino fluence as calculated in Section 2 ($\Gamma_{\rm jet} = 300$) with a significance of 4σ or larger is about 6%.

3.4. Results and Systematic Uncertainties

After all parameters of the analysis have been fixed, the on-time data are unblinded and analyzed with respect to two time windows.[44] The shorter one (from $T_0 - 3.8$ s to $T_0 + 62.2$ s)

[44] The time windows define the flat part of the signal time PDFs.

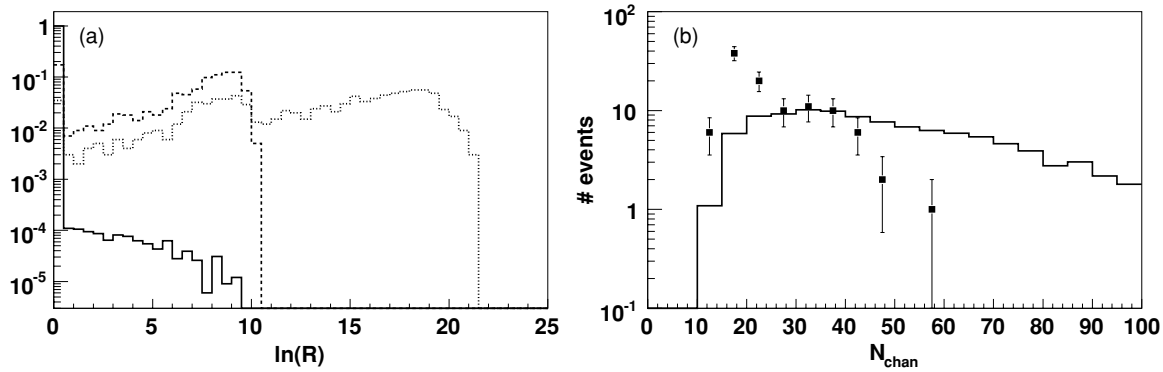

Figure 7. (a) Likelihood ratio distributions for background-only (off-time) data sets (solid line) and for the same background data sets with one (dashed line) and two (dotted line) signal events injected. (b) $N_{\rm chan}$ distributions for off-time data (squares), and signal Monte Carlo (solid line) after final cuts. Data events are selected within a radius of 20° around the GRB position. The Monte Carlo has been normalized to the number of events in data.

corresponds to the immediate emission time of the γ-rays, whereas the second (from $T_0 - 173$ s to $T_0 + 130$ s) covers the whole time range with IceCube data (see Figure 2). No significant deviation from the background-only hypothesis was found in either of the two time windows. In both cases, the unbinned likelihood method yields $\ln(\mathcal{R}(\langle\hat{n}_s\rangle)) = 0$ with $\langle\hat{n}_s\rangle = 0$ as the best estimate for the number of signal events. The resulting Neyman 90% CL upper limit (Neyman 1937; Amsler et al. 2008) on the number of signal events in the short time window is 2.7, i.e., injecting signal events according to a Poisson distribution with mean 2.7 into the on-time data yields $\ln(\mathcal{R}(\langle\hat{n}_s\rangle)) > 0$ in 90% of cases. From the neutrino fluence calculated in Section 2 for $\Gamma_{\rm jet} = 300$, we expect to see 0.1 events. This results in a model rejection factor (MRF; Hill & Rawlins 2003) of 27 which is defined as the ratio between the upper limit on the number of signal events and the expected number of signal events. The corresponding upper limit on the muon neutrino fluence is plotted in Figure 8(a) in the energy range containing 90% of the detected signal events. Integrating the fluence over this energy range yields an upper limit of 9.5×10^{-3} erg cm^{-2}. This upper limit is slightly conservative as we do not consider the effect of ν_τ from GRBs. Tau neutrinos might manifest themselves as τ tracks (which can travel a substantial distance at PeV energies) or as muons from tau decays.[45] The impact of a larger bulk Lorentz boost on the MRF is displayed in Figure 8(b). In addition, the MRFs for $\Gamma_{\rm jet} = 500$ and 1400 are listed in Table 3.

The effects of systematic errors on the result, described below in detail, were investigated by varying simulation parameters and repeating the full analysis. The quadratic sum of all systematic errors is (+17%, −4%). The main sources of systematic uncertainty are as follows.

Ice simulation. Inaccuracies in the ice simulation can lead to a wrong estimate of the efficiency of the detector to neutrinos from the GRB. In order to estimate the size of this effect, the analysis was repeated using a modified ice simulation. In this simulation, the DOM efficiency was altered as a function of depth according to the differences observed between data and Monte Carlo in the DOM occupancy, effectively making the ice clearer for depths with above-average transparencies and dirtier for depths with below-average transparencies. This leads to an increase of the fluence upper limit of 16%, which is included as a one-sided systematic error (see "DOM efficiency").

[45] Electron neutrinos do not contribute to the signal as the resulting electron immediately produces an electromagnetic cascade.

DOM efficiency. Uncertainties in the efficiency of the optical modules in the photon detection lead to an uncertainty in the number of expected events from the GRB. Varying the efficiency by ±10% changes the upper limit by ±4%;

Background rate. Even after optimized cuts, the data set is dominated by misreconstructed downgoing atmospheric muons. The rate varies throughout the year due to changes in the density profile of the atmosphere at high altitude above the South Pole by about 10% around the mean value. As the number of events after cuts in the data set during the GRB is too low, the rate at the time of the GRB was determined using a 1 hr data set recorded with the same DAQ settings about a week later. In order to account for potential differences, the background data rate was varied by ±10%. This results in a shift of the upper limit of less than ±1%.

4. COMPARISON WITH OTHER RESULTS

In Murase (2008), the author calculates neutrino spectra for a burst like GRB 080319B with different models. The expected fluences in the best cases are below our optimistic scenario. Therefore, our limits do not constraint these models.

In Thrane et al. (2009), the Super-Kamiokande collaboration reports on upper limits on the neutrino fluence from GRB 080319B. They analyzed their data in different energy ranges between ∼100 MeV and ∼1 TeV. Their strongest fluence limits come from the high-energy *upmu* data set and amount to 16 cm^{-2} (22 cm^{-2}) at 90% CL for (anti) muon neutrinos assuming an E^{-2} spectrum. In comparison, IceCube reaches an upper limit of 1.1×10^{-5} cm^{-2} in the energy range $E_\nu = 120$ TeV–2.2 PeV. A direct comparison of the results is difficult as the Super-Kamiokande paper does not contain information about the neutrino energy integration range used in the calculation of the limits. Assuming a lower integration boundary of $E_{\nu,1} = 10$ GeV and an upper boundary $E_{\nu,2} \gg E_{\nu,1}$ yields a sensitivity for an E^{-2} spectrum that is about 200 times worse than that of IceCube (for equal fluxes of muon and anti muon neutrinos).

Along with high-energy neutrinos which origin from the decay of charged pions high-energy γ-ray photons are produced in the decay of simultaneously generated neutral pions. In addition, high-energy photons are produced in inverse Compton scattering of synchrotron photons by accelerated electrons (Falcone et al. 2008). In contrast to neutrinos, the flux of high-energy γ-ray photons at the Earth is significantly reduced due to the large optical depths for photon–photon pair production

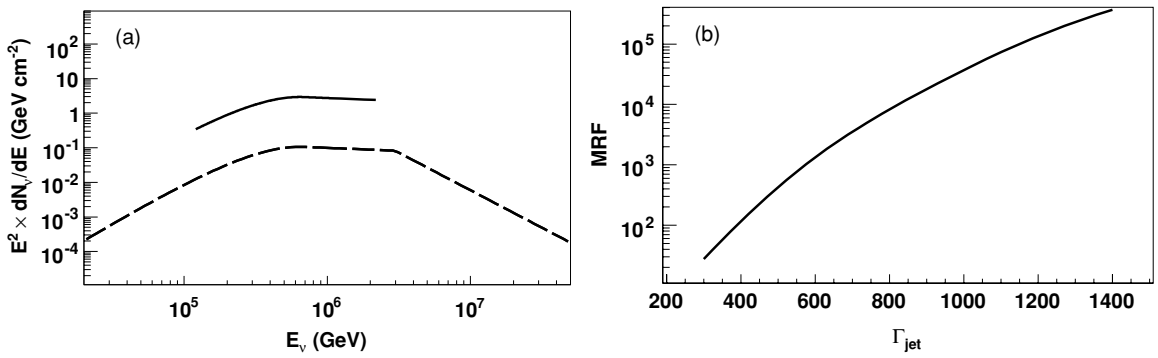

Figure 8. (a) Ninety percent CL upper limit on the fluence from GRB 080319B (solid line) with respect to the calculated neutrino fluence for a bulk Lorentz boost of the jet of $\Gamma_{jet} = 300$ (dashed line). (b) Ratio between upper limit and calculated fluence spectrum (MRF) as a function of Γ_{jet}.

Table 3
Neutrino Spectrum Parameters According to the Fireball Model for GRB 080319B for Different Bulk Lorentz Factors of the Jet Together with the Expected Mean Number of Events in the Detector and the Model Rejection Factor Obtained from the Analysis

Parameter\bulk Lorentz factor	$\Gamma_{jet} = 300$	$\Gamma_{jet} = 500$	$\Gamma_{jet} = 1400$
1st break energy, ϵ_1	260 TeV	710 TeV	5.6 PeV
2nd break energy, ϵ_2	3 PeV	23 PeV	1.4 EeV
1st index, α_ν	0.5	0.5	0.5
2nd index, β_ν	2.17	2.17	2.17
3rd index, γ_ν	4.17	4.17	4.17
Fluence at 1st break energy	7.3×10^{-13} GeV^{-1} cm^{-2}	1.4×10^{-14} GeV^{-1} cm^{-2}	2.9×10^{-18} GeV^{-1} cm^{-2}
Expected events in IceCube	0.10	8.6×10^{-3}	9.6×10^{-6}
MRF	27	420	3.7×10^5

inside the source for not too large jet Lorentz factors $\Gamma_{jet} \lesssim 800$ (Falcone et al. 2008). In addition, high-energy photons above 100 GeV are absorbed on the extragalactic background light if they travel distances $z \gtrsim 0.5$. Observations with air-Cherenkov telescopes like H.E.S.S. (Aharonian et al. 2009; Tam et al. 2009) or MAGIC (Albert et al. 2007; Galante et al. 2009) are also hampered by the fact that usually it takes more than 50 s (MAGIC) or 100 s (H.E.S.S.) from the observation of a GRB by a satellite to the start of data taking with these telescopes. Therefore, the prompt emission window is only partially covered or not at all. Milagro (Atkins et al. 2004; Abdo et al. 2007) as an air shower array observed the visible sky continuously. However, it was mostly sensitive to energies above 1 TeV. Up to now, there has been no definitive detection of very high energy γ-ray emission from GRBs. Milagrito (Atkins et al. 2000, 2003) and the HEGRA AIROBICC array (Padilla et al. 1998) reported evidence at the 3σ level for high-energy γ-ray emission from GRB 970417A ($E_\gamma > 650$ GeV) and GRB 920925C ($E_\gamma > 20$ TeV), respectively. However, subsequent searches for high-energy gamma ray emission from GRBs did not find similar signals. For GRB 080319B, no high-energy γ-ray data exist (MAGIC, which has a threshold below 100 GeV, was not able to observe the burst as it was already dawning; E. Lorenz 2008, private communication). Current flux predictions are near or below the sensitivity of current instruments (Falcone et al. 2008), where the predicted fluxes in the energy range below ~100 TeV are dominated by the leptonic emission component in most scenarios. Therefore, the upper limits from high-energy γ-ray observations do not constrain the neutrino flux in our model or the computed upper limit.

5. CONCLUSIONS AND OUTLOOK

We used the IceCube neutrino telescope to search for high-energy muon neutrinos from GRB 080319B, one of the most spectacular and well-measured GRBs ever observed. Based on the fireball model of GRBs and the measured γ-ray fluence, we calculated the expected neutrino spectrum for different jet bulk Lorentz boosts Γ_{jet}. After applying quality cuts to suppress misreconstructed atmospheric muons, a mean number of 0.1 signal events is expected for the optimistic case of $\Gamma_{jet} = 300$ (for other Γ_{jet} see Table 3) in IceCube, which was running in a nine-string configuration. The data were analyzed with an unbinned log-likelihood method utilizing the directional and temporal distance of reconstructed tracks to the GRB. The sensitivity to a potential GRB signal was enhanced by evaluating energy information. No deviation from the background-only hypothesis was found either in a small time window covering the immediate γ-ray emission time or an extended window of 300 s. This results in a 90% CL upper limit on the muon neutrino fluence from GRB 080319B within the short time window of 9.5×10^{-3} erg cm^{-2} in the energy range between 120 TeV and 2.2 PeV which contains 90% of the expected signal events. The corresponding ratio between the upper limit and the calculated GRB spectrum (MRF) is 27. Its stability with respect to systematic uncertainties in the analysis is estimated to be (+17%, −4%). The upper limit does not allow us to impose constraints on GRB parameters within the fireball model.

In its final configuration with 80 strings, the expected number of detected events in IceCube from a bright GRB like GRB 080319B is $\mathcal{O}(1)$, rendering the individual analysis of these rare GRBs highly interesting also in the future. Using the large number of GRBs observed by the *Swift* and *Fermi* (formerly *GLAST*) satellites, the growing IceCube detector will also soon be able to probe the Waxman–Bahcall or similar GRB fluxes and in the case of a non-detection set stringent limits.

We acknowledge the support from the following agencies: U.S. National Science Foundation-Office of Polar Program, U.S.

National Science Foundation-Physics Division, University of Wisconsin Alumni Research Foundation, U.S. Department of Energy, and National Energy Research Scientific Computing Center, the Louisiana Optical Network Initiative (LONI) grid computing resources; Swedish Research Council, Swedish Polar Research Secretariat, and Knut and Alice Wallenberg Foundation, Sweden; German Ministry for Education and Research (BMBF), Deutsche Forschungsgemeinschaft (DFG), Germany; Fund for Scientific Research (FNRS-FWO), Flanders Institute to encourage scientific and technological research in industry (IWT), Belgian Federal Science Policy Office (Belspo); the Netherlands Organisation for Scientific Research (NWO); Marsden Fund, New Zealand; M.R. acknowledges the support of the SNF (Switzerland); A.K. and A.G. acknowledge support by the EU Marie Curie OIF Program; J.P.R. acknowledge support by the Capes Foundation, Ministry of Education of Brazil.

APPENDIX

EQUATIONS USED IN THE CALCULATION OF THE NEUTRINO SPECTRUM

$$F_\gamma(E_\gamma) = \frac{dN(E_\gamma)}{dE_\gamma}, \tag{A1}$$

$$= f_\gamma \times \begin{cases} \left(\frac{E_\gamma}{\mathrm{MeV}}\right)^{-\alpha_\gamma} \exp\left(-\frac{E_\gamma}{\epsilon_\gamma}\right) & \text{for } E_\gamma < \epsilon_\gamma \\ \left(\frac{E_\gamma}{\mathrm{MeV}}\right)^{-\beta_\gamma} \left[(\beta_\gamma - \alpha_\gamma)\frac{\epsilon_\gamma}{\mathrm{MeV}}\right]^{\beta_\gamma - \alpha_\gamma} & \\ \quad \times \exp(\alpha_\gamma - \beta_\gamma) & \text{for } E_\gamma \geqslant \epsilon_\gamma, \end{cases} \tag{A2}$$

$$\mathcal{F}_\gamma = \int_{20\ \mathrm{keV}}^{7\ \mathrm{MeV}} dE_\gamma\ E_\gamma F_\gamma(E_\gamma), \tag{A3}$$

$$F_\nu(E_\nu) = \frac{dN(E_\nu)}{dE_\nu}, \tag{A4}$$

$$= f_\nu \times \begin{cases} \left(\frac{E_\nu}{\mathrm{GeV}}\right)^{-\alpha_\nu} \exp\left(-\frac{E_\nu}{\epsilon_1}\right) & \text{for } E_\nu < \epsilon_1 \\ \left(\frac{E_\nu}{\mathrm{GeV}}\right)^{-\beta_\nu} \left[(\beta_\nu - \alpha_\nu)\frac{\epsilon_1}{\mathrm{GeV}}\right]^{\beta_\nu - \alpha_\nu} & \\ \quad \times \exp(\alpha_\nu - \beta_\nu) & \text{for } \epsilon_1 \leqslant E_\nu < \epsilon_2 \\ \left(\frac{E_\nu}{\mathrm{GeV}}\right)^{-\gamma_\nu} \left[(\beta_\nu - \alpha_\nu)\frac{\epsilon_1}{\mathrm{GeV}}\right]^{\beta_\nu - \alpha_\nu} & \\ \quad \times \exp(\alpha_\nu - \beta_\nu)\left(\frac{\epsilon_2}{\mathrm{GeV}}\right)^{-\beta_\nu} & \text{for } E_\nu \geqslant \epsilon_2, \end{cases} \tag{A5}$$

$$\epsilon_1 = 7.5 \times 10^5\ \mathrm{GeV}\ \frac{1}{(1+z)^2}\left(\frac{\Gamma_{\mathrm{jet}}}{10^{2.5}}\right)^2\left(\frac{\mathrm{MeV}}{\epsilon_\gamma}\right), \tag{A6}$$

$$\epsilon_2 = 10^7\,\mathrm{GeV}\ \frac{1}{1+z}\sqrt{\frac{\epsilon_e}{\epsilon_B}}\left(\frac{\Gamma_{\mathrm{jet}}}{10^{2.5}}\right)^4\left(\frac{t_{\mathrm{var}}}{0.01\ \mathrm{s}}\right)\sqrt{\frac{10^{52}\ \mathrm{erg\ s^{-1}}}{L_\gamma^{\mathrm{iso}}}}, \tag{A7}$$

$$\alpha_\nu = 3 - \beta_\gamma, \quad \beta_\nu = 3 - \alpha_\gamma, \quad \gamma_\nu = \beta_\nu + 2, \tag{A8}$$

$$\frac{\Delta R}{\lambda_{p\gamma}} = \left(\frac{L_\gamma^{\mathrm{iso}}}{10^{52}\ \mathrm{erg\ s^{-1}}}\right)\left(\frac{0.01\ \mathrm{s}}{t_{\mathrm{var}}}\right)\left(\frac{10^{2.5}}{\Gamma_{\mathrm{jet}}}\right)^4\left(\frac{\mathrm{MeV}}{\epsilon_\gamma}\right), \tag{A9}$$

$$\int_0^\infty dE_\nu E_\nu F_\nu(E_\nu) = \frac{1}{8}\frac{1}{f_e}\left(1 - (1 - \langle x_{p\to\pi}\rangle)^{\Delta R/\lambda_{p\gamma}}\right) \times \int_0^\infty dE_\gamma\ E_\gamma F_\gamma(E_\gamma). \tag{A10}$$

The parameters of the γ-ray spectrum $F_\gamma(E_\gamma)$ are the break energy ϵ_γ and the spectrum indices before and after the break α_γ and β_γ, respectively. The quantity $\mathcal{F}_\gamma$ is the measured γ-ray fluence and z the redshift of the GRB. The parameters of the neutrino spectrum $F_\nu(E_\nu)$ are the two break energies, ϵ_1 and ϵ_2, and the corresponding spectral indices α_ν, β_ν, and γ_ν. The expression $1-(1-\langle x_{p\to\pi}\rangle)^{\Delta R/\lambda_{p\gamma}}$ in Equation (A10) estimates the overall fraction of the proton energy going into pions from the size of the shock, ΔR, and the mean free path of a proton for photomeson interactions, $\lambda_{p\gamma}$. Here, $\langle x_{p\to\pi}\rangle = 0.2$ is the average fraction of proton energy transferred to a pion in a single interaction. The expression ensures that the transferred energy fraction is $\leqslant 1$. The variables f_γ and f_ν are obtained from the integrals of Equations (A3) and (A10). The isotropic equivalent luminosity, L_γ^{iso}, is given by the isotropic equivalent energy released in γ-rays, E_γ^{iso}, divided by the burst duration. The calculations are insensitive to the beaming effect caused by a narrow opening angle of the jet (0.°4 for GRB 080319B according to Racusin et al. 2008a) as all formulae contain the isotropic luminosity in conjunction with a 4π shell geometry, i.e., effectively use luminosity per steradian. For example, the target photon density used to calculate $\lambda_{p\gamma}$ is given by $n_\gamma \propto L_\gamma^{\mathrm{iso}}/4\pi R^2$.

REFERENCES

Abbasi, R., et al. (IceCube Collaboration) 2009, Nucl. Inst. Meth. A, 601, 294
Abdo, A. A., et al. (Milagro Collaboration) 2007, ApJ, 666, 361
Achterberg, A., et al. (IceCube Collaboration) 2006, Astropart. Phys., 26, 155
Achterberg, A., et al. (IceCube Collaboration) 2007, ApJ, 664, 397
Achterberg, A., et al. (IceCube Collaboration) 2008, ApJ, 674, 357
Ackermann, M., et al. (AMANDA Collaboration) 2006, J. Geophys. Res., 111, D13203
Aharonian, F., et al. (H.E.S.S. Collaboration) 2009, ApJ, 690, 1068
Ahrens, J., et al. (AMANDA Collaboration) 2004, Nucl. Inst. Meth. A, 524, 169
Albert, J., et al. (MAGIC Collaboration) 2007, ApJ, 667, 358
Alvarez-Muniz, J., & Halzen, F. 1999, ApJ, 521, 928
Alvarez-Muniz, J., Halzen, F., & Hooper, D. W. 2000, Phys. Rev. D, 62, 093015
Amsler, C., et al. 2008, Phys. Lett. B, 667, 1
Atkins, R. W., et al. (Milagro Collaboration) 2000, ApJ, 533, L119
Atkins, R. W., et al. (Milagro Collaboration) 2003, ApJ, 583, 824
Atkins, R. W., et al. (Milagro Collaboration) 2004, ApJ, 604, L25
Band, D., et al. 1993, ApJ, 413, 281
Barlow, R. J. 1989, Statistics (Chichester: Wiley)
Barr, G. D., et al. 2004, Phys. Rev. D, 70, 023006
Becker, J. K. 2008, Phys. Rep., 458, 173
Becker, J. K., Stamatikos, M., Halzen, F., & Rhode, W. 2006, Astropart. Phys., 25, 118
Braun, J., Dumm, J., de Palma, F., Finley, C., Karle, A., & Montaruli, T. 2008, Astropart. Phys., 29, 299
Burrows, D. N., et al. 2005, Space Sci. Rev., 120, 165
Chirkin, D., & Rhode, W. 2004, arXiv:hep-ph/0407075
Cwiok, M., et al. 2008, GRB 080319B Light Curve by Pi-of-the-Sky, http://gcn.gsfc.nasa.gov/gcn3/7445.gcn3
Falcone, A. D., et al. 2008, arXiv:0810.0520
Galante, N., et al. (MAGIC Collaboration) 2009, in AIP Conf. Proc. 1085, High Energy Gamma-ray Astronomy, ed. F. A. Aharonian, W. Hofmann, & F. Reiger (Melville, NY: AIP), 411
Gazizov, A., & Kowalski, M. O. 2005, Comp. Phys. Comm., 172, 203
Guetta, D., Hooper, D., Alvarez-Muniz, J., Halzen, F., & Reuveni, E. 2004, Astropart. Phys., 20, 429
Hill, G. C., & Rawlins, K. 2003, Astropart. Phys., 19, 393
Kashti, T., & Waxman, E. 2005, Phys. Rev. Lett., 95, 181101
Kumar, P., & Panaitescu, A. 2008, MNRAS, 391, L19
Lundberg, J., et al. 2007, Nucl. Inst. Meth. A, 581, 619
Margutti, R., et al. 2008, in AIP Conf. Proc. 1065, 2008 Nanjing Gamma-ray Burst Conf., ed. Y.-F. Huang, Z. G. Dai, & B. Zhang (Melville, NY: AIP), 259
Meszaros, P., & Rees, M. J. 1993, ApJ, 405, 278
Murase, K. 2008, Phys. Rev. D, 78, 101302
Murase, K., & Nagataki, S. 2006, Phys. Rev. D, 73, 063002

Narayan, R., Paczynski, B., & Piran, T. 1992, ApJ, 395, L83
NASA 1994, Konus-Wind Homepage, http://heasarc.gsfc.nasa.gov/docs/heasarc/missions/wind.html
Neyman, J. 1937, Phil. Trans. Roy. Soc., 236, 333
Padilla, L., et al. 1998, A&A, 337, 43
Pandey, S. B., et al. 2009, A&A, in press (arXiv:0904.1797)
Piran, T., Sari, R., & Zou, Y. 2009, Mon. Not. R. Astron. Soc., 393, 1107
Racusin, J. L., et al. 2008a, Nature, 455, 183
Racusin, J. L., et al. 2008b, Swift Observation of GRB 080319B, http://gcn.gsfc.nasa.gov/reports/report_134_1.pdf
Razzaque, S., Meszaros, P., & Waxman, E. 2003, Phys. Rev. Lett., 90, 241103
Rees, M. J., & Meszaros, P. 1994, ApJ, 430, L93
Sari, R., & Piran, T. 1997, ApJ, 485, 270
Stamatikos, M., et al. (IceCube Collaboration) 2005, in Proc. Int. Cosmic Ray Conf. (ICRC'05), Vol. 4, ed. B. Sripathi et al. (India: Tata Institute of Fundamental Research), 471
Tam, P., et al. (H.E.S.S. Collaboration) 2009, arXiv:0902.1561
Thrane, E., et al. (Super-Kamiokande Collaboration) 2009, ApJ, 697, 730
Vreeswijk, P. M., et al. 2008, VLT/UVES Redshift of GRB 080319B from FeII Fine-Structure Lines, http://gcn.gsfc.nasa.gov/gcn3/7451.gcn3
Waxman, E., & Bahcall, J. N. 1997, Phys. Rev. Lett., 78, 2292